Journal of Quantitative Spectroscopy & Radiative Transfer 100 (2006) 115–121

Journal of Quantitative Spectroscopy & Radiative Transfer

www.elsevier.com/locate/jqsrt

Enhanced backscattering of polarized light: Effect of particle nonsphericity on the helicity-preserving enhancement factor

Janna M. Dlugach[a], Michael I. Mishchenko[b,*]

[a]Main Astronomical Observatory of the National Academy of Sciences of Ukraine, 27 Zabolotny Str., 03680 Kyiv, Ukraine
[b]NASA Goddard Institute for Space Studies, 2880 Broadway, New York, NY 10025, USA

Abstract

We analyze theoretically the effect of particle nonsphericity on the backscattering enhancement factor ζ_{hp} in the helicity-preserving channel. Using numerically exact *T*-matrix and vector radiative-transfer codes, we have performed computations for optically semi-infinite homogeneous layers composed of polydisperse, randomly oriented oblate spheroids with the real part of the refractive index equal to 1.2, 1.4, and 1.6, the imaginary part of the refractive index equal to 0 and 0.01, various values of the equal-surface-area-sphere effective size parameter, and aspect ratios $1 \leqslant \varepsilon \leqslant 2$. Our computations demonstrate that whereas for spheres $\zeta_{hp} \equiv 2$, for spheroids the helicity-preserving enhancement factor can deviate quite significantly from the value 2. The magnitude of this deviation varies substantially with particle microphysical parameters and illumination geometry.

Keywords: Enhancement factor; Coherent backscattering; Polarization; Nonspherical particles

1. Introduction

During the past two decades, extensive experimental and theoretical studies of coherent backscattering (CB) of polarized light from discrete disordered media have been reported (see, e.g. [1–9] and references therein). Initially, various approximate methods were used in theoretical analyses of this problem (see, e.g. [10–15]). More recently, Mishchenko [16,17] has used the microscopic vector theory of CB [9] to derive rigorous relations for the computation of various polarization enhancement factors in the case of the exact backscattering direction for media composed of independently scattering particles of arbitrary size and shape. General properties of these characteristics have been studied, and the results of computations, performed mainly for spherical particles, have been reported [18,19].

It is interesting and important, however, to examine in detail how the enhancement factors can be affected by particle nonsphericity, which is exactly the purpose of this paper. We present and analyze the results of computations of the helicity-preserving enhancement factor, ζ_{hp}, for semi-infinite homogeneous slabs composed of polydisperse, randomly oriented oblate spheroids with varying aspect ratios. The interest in this

*Corresponding author. Tel.: +1 212 678 5590; fax: +1 212 678 5622.
E-mail address: crmim@giss.nasa.gov (M.I. Mishchenko).

0022-4073/$ - see front matter
doi:10.1016/j.jqsrt.2005.11.060

problem stems partially from the fact that in the case of spherical particles $\zeta_{\text{hp}} \equiv 2$, whereas the results of laboratory measurements of ζ_{hp} reported in [20] showed a notable deviation from the value 2, which was interpreted in terms of a significant contribution of recurrent multiple scattering to the reflected light. We will demonstrate that these laboratory results may allow an alternative interpretation.

2. Basic formulae

Let the scattering medium be a plane-parallel semi-infinite slab composed of randomly distributed, independently scattering particles. This slab is illuminated by a parallel beam of light incident in the direction specified by a couplet $\{\theta \geqslant \pi/2, \varphi = 0\}$, and $\boldsymbol{\mathscr{R}}$ is the Stokes reflection matrix for exactly the backscattering direction $\{\pi - \theta, \pi\}$. The θ and φ are the polar and azimuth angles, respectively, specified in a spherical coordinate system with the z-axis oriented along the outward normal to the boundary of the slab. We will also specify the direction of incidence by the couplet $\{\mu \geqslant 0, \varphi = 0\}$, where $\mu = -\cos\theta$.

For a macroscopically isotropic and mirror-symmetric scattering medium [9,21,22], the matrix $\boldsymbol{\mathscr{R}}$ has the following block-diagonal structure:

$$\boldsymbol{\mathscr{R}} = \begin{bmatrix} \mathscr{R}_{11} & \mathscr{R}_{12} & 0 & 0 \\ \mathscr{R}_{12} & \mathscr{R}_{22} & 0 & 0 \\ 0 & 0 & \mathscr{R}_{33} & \mathscr{R}_{34} \\ 0 & 0 & -\mathscr{R}_{34} & \mathscr{R}_{44} \end{bmatrix}. \tag{1}$$

In accordance with the microscopic theory of coherent backscattering [9], the matrix $\boldsymbol{\mathscr{R}}$ can be decomposed as

$$\boldsymbol{\mathscr{R}} = \boldsymbol{\mathscr{R}}^1 + \boldsymbol{\mathscr{R}}^{\text{M}} + \boldsymbol{\mathscr{R}}^{\text{C}}, \tag{2}$$

where $\boldsymbol{\mathscr{R}}^1$ is the contribution of the first-order scattering, $\boldsymbol{\mathscr{R}}^{\text{M}}$ is the diffuse multiple-scattering contribution composed of all the ladder diagrams of orders $n \geqslant 2$, and $\boldsymbol{\mathscr{R}}^{\text{C}}$ is the cumulative contribution of all the cyclical diagrams. The matrices $\boldsymbol{\mathscr{R}}^1$ and $\boldsymbol{\mathscr{R}}^{\text{M}}$ can be found by solving the vector form of the Ambarzumian's nonlinear integral equation [9,16,19,23]. Then the matrix $\boldsymbol{\mathscr{R}}^{\text{C}}$ can be obtained from the following exact relation [17]:

$$\boldsymbol{\mathscr{R}}^{\text{C}} = \begin{bmatrix} \mathscr{R}^{\text{C}}_{11} & \mathscr{R}^{\text{M}}_{12} & 0 & 0 \\ \mathscr{R}^{\text{M}}_{12} & \mathscr{R}^{\text{C}}_{22} & 0 & 0 \\ 0 & 0 & \mathscr{R}^{\text{C}}_{33} & \mathscr{R}^{\text{M}}_{34} \\ 0 & 0 & -\mathscr{R}^{\text{M}}_{34} & \mathscr{R}^{\text{C}}_{44} \end{bmatrix}, \tag{3}$$

where

$$\mathscr{R}^{\text{C}}_{11} = \tfrac{1}{2}(\mathscr{R}^{\text{M}}_{11} + \mathscr{R}^{\text{M}}_{22} - \mathscr{R}^{\text{M}}_{33} + \mathscr{R}^{\text{M}}_{44}), \tag{4}$$

$$\mathscr{R}^{\text{C}}_{22} = \tfrac{1}{2}(\mathscr{R}^{\text{M}}_{11} + \mathscr{R}^{\text{M}}_{22} + \mathscr{R}^{\text{M}}_{33} - \mathscr{R}^{\text{M}}_{44}), \tag{5}$$

$$\mathscr{R}^{\text{C}}_{33} = \tfrac{1}{2}(-\mathscr{R}^{\text{M}}_{11} + \mathscr{R}^{\text{M}}_{22} + \mathscr{R}^{\text{M}}_{33} + \mathscr{R}^{\text{M}}_{44}), \tag{6}$$

$$\mathscr{R}^{\text{C}}_{44} = \tfrac{1}{2}(\mathscr{R}^{\text{M}}_{11} - \mathscr{R}^{\text{M}}_{22} + \mathscr{R}^{\text{M}}_{33} + \mathscr{R}^{\text{M}}_{44}). \tag{7}$$

For sparsely distributed, independently scattering particles, the Stokes scattering matrix is independent of the particle number density [9].

For circularly polarized incident light with a Stokes column vector $\mathbf{I}_0 = [I_0\,0\,0\,I_0]^{\text{T}}$, the backscattering enhancement factor in the helicity-preserving channel is as follows [17]:

$$\begin{aligned} \zeta_{\text{hp}} &= \frac{\mathscr{R}^1_{11} + \mathscr{R}^1_{44} + 2\mathscr{R}^{\text{M}}_{11} + 2\mathscr{R}^{\text{M}}_{44}}{\mathscr{R}^1_{11} + \mathscr{R}^1_{44} + \mathscr{R}^{\text{M}}_{11} + \mathscr{R}^{\text{M}}_{44}} \\ &= 1 + \frac{\mathscr{R}^{\text{M}}_{11} + \mathscr{R}^{\text{M}}_{44}}{\mathscr{R}^1_{11} + \mathscr{R}^1_{44} + \mathscr{R}^{\text{M}}_{11} + \mathscr{R}^{\text{M}}_{44}}. \end{aligned} \tag{8}$$

For spherically symmetric scatterers, $\mathscr{R}^1_{44} = -\mathscr{R}^1_{11}$ so that $\zeta_{hp} \equiv 2$, whereas for randomly oriented nonspherical particles $1 \leqslant \zeta_{hp} \leqslant 2$. For grazing incidence and/or a small single-scattering albedo ϖ, the main contribution to the backscattered diffuse radiation comes from the singly scattered light. This means that with $\mu \to 0$ and/or with $\varpi \to 0$, the diffuse multiple-scattering component of the Stokes reflection matrix $\mathscr{R}^{M}$ decreases and ultimately vanishes in comparison with the first-order-scattering component, and we have

$$\lim_{\mu \to 0} \zeta_{hp} = 1, \tag{9}$$

$$\lim_{\varpi \to 0} \zeta_{hp} = 1. \tag{10}$$

The results of computations reported in [17] for one model of monodisperse oblate spheroids showed perfect numerical agreement with the theoretical limit (9).

To determine the elements of the matrix $\mathscr{R}^{M}$, one must first calculate the elements of the normalized Stokes scattering matrix for the particles forming the medium [9,21,22]. In this study, we have used the exact method that was developed in [24] and is based on Waterman's T-matrix approach [25]. Then the elements $\mathscr{R}^{M}_{11}$ and $\mathscr{R}^{M}_{44}$ were computed by means of a numerical solution of Ambarzumian's nonlinear integral equation as described in [19,23].

3. Numerical results and discussion

To model the potential effect of particle nonsphericity on the helicity-preserving enhancement factor ζ_{hp}, we have chosen randomly oriented oblate spheroids distributed over surface-equivalent-sphere radii r according to the following power law:

$$n(r) = \begin{cases} \text{constant} \times r^{-3}, & r_1 \leqslant r \leqslant r_2, \\ 0 & \text{otherwise.} \end{cases} \tag{11}$$

The effective radius and effective variance of the size distribution are defined by

$$r_{\text{eff}} = \frac{1}{\langle G \rangle} \int_{r_1}^{r_2} \mathrm{d}r\, n(r) r \pi r^2, \tag{12}$$

$$v_{\text{eff}} = \frac{1}{\langle G \rangle r_{\text{eff}}^2} \int_{r_1}^{r_2} \mathrm{d}r\, n(r)(r - r_{\text{eff}})^2 \pi r^2, \tag{13}$$

respectively, where

$$\langle G \rangle = \int_{r_1}^{r_2} \mathrm{d}r\, n(r) \pi r^2 \tag{14}$$

is the average area of the geometrical projection per particle [21]. The shape of a spheroid is fully described by just one parameter, the aspect ratio ε (i.e., the ratio of the larger to the smaller spheroid axes), along with a designation of either prolate or oblate.

We have performed computations of the helicity-preserving enhancement factor for a semi-infinite homogeneous slab composed of spheroids with the real part of the refractive index $\mathsf{m}_R = 1.2, 1.4$, and 1.6, the imaginary part of the refractive index $\mathsf{m}_I = 0$ and 0.01, a range of values of the effective size parameter $x_{\text{eff}} = 2\pi r_{\text{eff}}/\lambda_1$ (λ_1 is the wavelength of the incident radiation in the surrounding medium), and aspect ratios $1 \leqslant \varepsilon \leqslant 2$. The effective variance of the size distribution v_{eff} was fixed at 0.1. The main results of our computations are shown in the form of color diagrams of the helicity-preserving enhancement factor as a function of the effective size parameter and aspect ratio for $\mu = 1, 0.642$, and 0.008, Figs. 1 and 2.

Let us first analyze the case of conservative scattering, $\mathsf{m}_I = 0$. Fig. 1 reveals a significant dependence of ζ_{hp} on the real part of the refractive index and illumination geometry. One can see that in the case of $\mathsf{m}_R = 1.2$ and normal incidence ($\mu = 1$), ζ_{hp} does not deviate substantially from the value 2 for all values of x_{eff} and ε considered. The reason for this is twofold: $\mathscr{R}^{M}_{44} \approx -\mathscr{R}^{M}_{11}$ for small effective size parameters, whereas $\mathscr{R}^1_{11} + \mathscr{R}^1_{44} \ll \mathscr{R}^{M}_{11} + \mathscr{R}^{M}_{44}$ for $x_{\text{eff}} \gtrsim 2$ [cf. Eq. (8)].

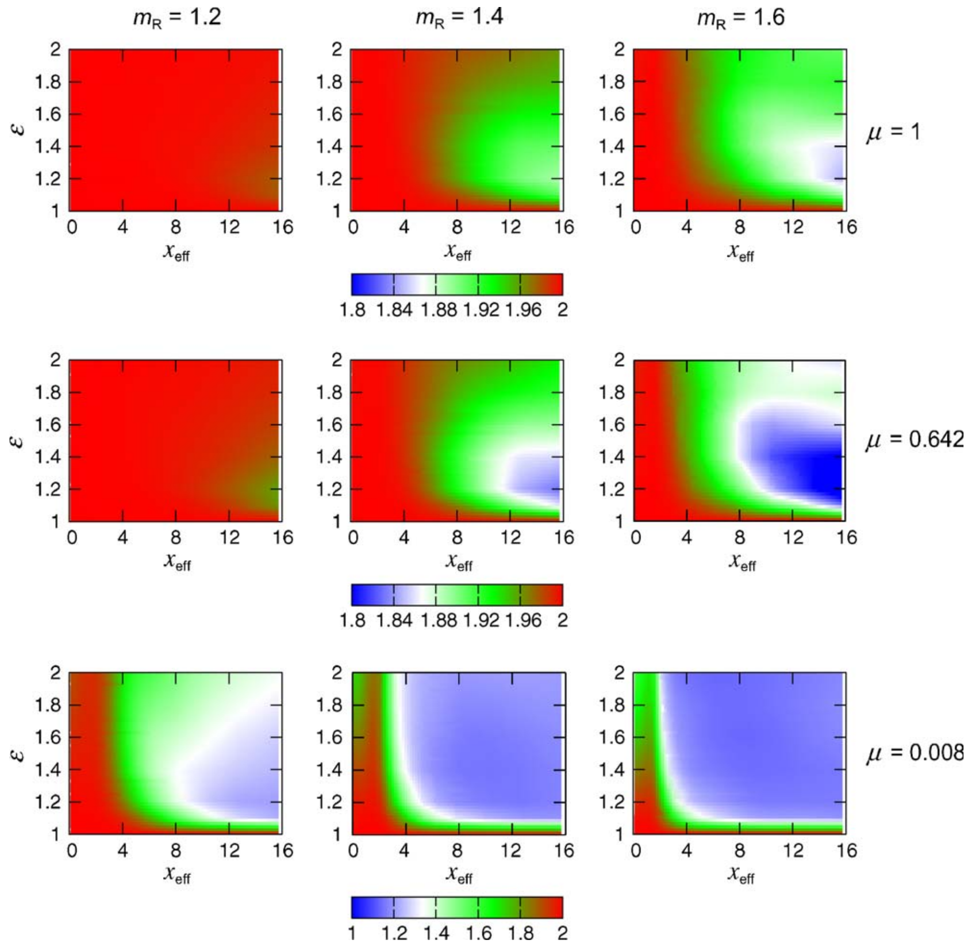

Fig. 1. Helicity-preserving enhancement factor versus effective equal-surface-area-sphere size parameter and aspect ratio for $m_R = 1.2$ (left-hand column), 1.4 (middle column), and 1.6 (right-hand column), and $\mu = 1$ (top row), 0.642 (middle row), and 0.008 (bottom row). The imaginary part of the refractive index is fixed at $m_I = 0$.

With a few exceptions, the deviation of the helicity-preserving enhancement factor from the value 2 increases with increasing real part of the refractive index and/or with increasing effective size parameter, which is a consequence of an increase in the first-order-scattering contribution and in the deviation of $\mathscr{R}_{44}^{M}$ from $-\mathscr{R}_{11}^{M}$. The range of effective size parameters at which the deviation of ζ_{hp} from the value 2 is significant also increases with increasing refractive index.

Interestingly, the helicity-preserving enhancement factor is not a monotonous function of the aspect ratio. This is a direct consequence of the specific aspect-ratio dependence of the elements $\mathscr{R}_{11}^{1}$ and $\mathscr{R}_{44}^{1}$ first observed and analyzed in [26]. Accordingly, Fig. 1 shows that with decreasing μ and, thus, with increasing contribution of the first-order scattering, the dependence of ζ_{hp} on particle asphericity increases and the value of ζ_{hp} decreases.

The bottom three diagrams of Fig. 1 are, perhaps, the most interesting in that they reveal an extremely complex interplay between the various parameters affecting the value of the helicity-preserving enhancement factor. Interestingly, even the illumination direction corresponding to $\mu = 0.008$ (i.e., $\theta - 90^\circ = 0.5^\circ$) is not grazing enough to make the multiple-scattering contribution much smaller than the single-scattering one, especially for $m_R = 1.2$.

The most obvious effect of increasing absorption is to reduce the single-scattering albedo, especially for very small particles [21], and hence the multiple-scattering contribution to the reflection matrix. The net result is a

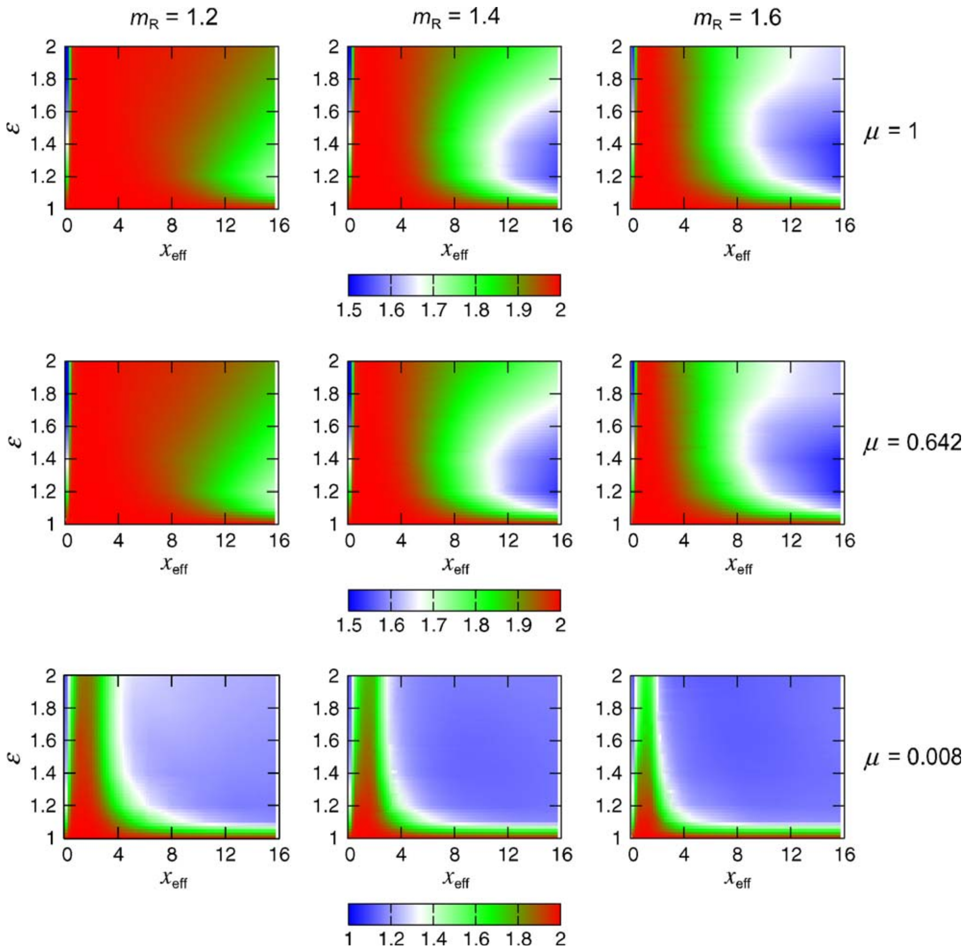

Fig. 2. As in Fig. 1, but for $m_I = 0.01$.

significant decrease in the helicity-preserving enhancement factor and a somewhat weaker dependence on illumination geometry, as demonstrated in Fig. 2. Fig. 3 details the effect of absorption on particles with very small size parameters and demonstrates how close to unity can ζ_{hp} be even in the case of normal incidence.

It should be noted that accurate numerical computations of the helicity-preserving enhancement factor become problematic for absorbing particles with vanishing size parameters since both the single-scattering and the multiple-scattering components of the reflection matrix become very small, thereby resulting in an ill-defined ratio on the right-hand side of Eq. (8). Therefore, the computation of the single-scattering matrix followed by the numerical solution of the radiative transfer equation must be carried out with maximal precision. Note that a similar problem, concerning the case of spherical particles, was discussed earlier in [19].

4. Conclusions

Using the model of a semi-infinite homogeneous slab composed of randomly oriented, polydisperse oblate spheroids with varying aspect ratios, we have demonstrated that the helicity-preserving enhancement factor can be affected profoundly by particle nonsphericity. Instead of being identically equal to 2, as is the case with spherically symmetric scatterers, the actual value of ζ_{hp} for nonspherical particles is the result of an intricate interplay of such factors as shape, real and imaginary parts of the refractive index, particle size, and illumination geometry.

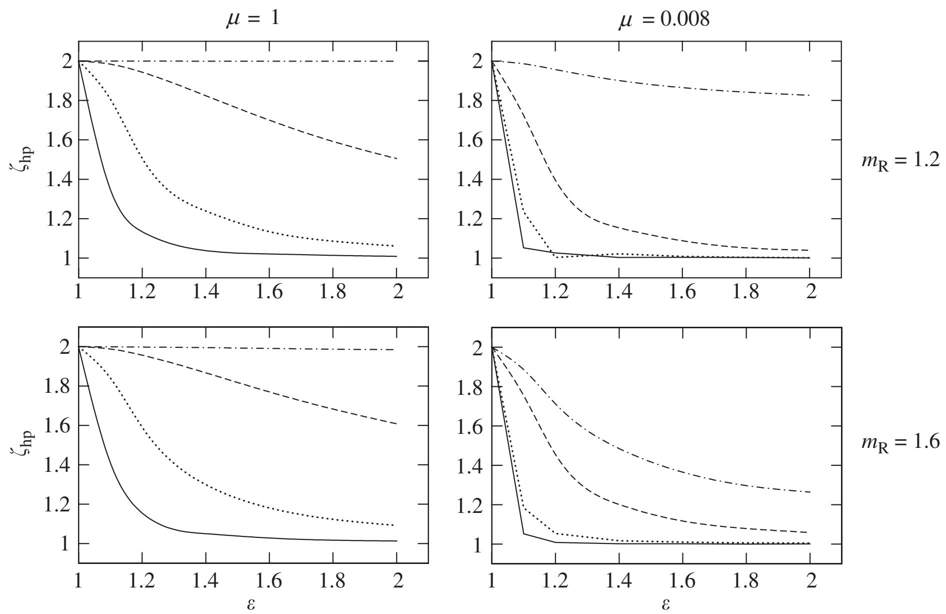

Fig. 3. Helicity-preserving enhancement factor versus aspect ratio for absorbing ($m_I = 0.01$) spheroids with $m_R = 1.2$ (top panels) and 1.6 (bottom panels). The incidence angles are those for and $\mu = 1$ (left-hand panels) and 0.008 (right-hand panels). Solid curves: $x_{eff} = 0.031$; dotted curves: $x_{eff} = 0.063$; dashed curves: $x_{eff} = 0.157$; dot-dashed curves: $x_{eff} = 2.09$.

Our numerical data exhibit ζ_{hp} values comparable to and even smaller than those reported by Wiersma et al. [20]. We thus may conclude that those experimental results can be explained, at least partially, by the fact that the solid particles that formed the laboratory scattering samples had nonspherical shapes. Unfortunately, the lack of precise and comprehensive microphysical characterization of the scattering particles in [20] makes it rather problematic to perform a definitive quantitative analysis of those measurement results.

Acknowledgement

This research was sponsored by the NASA Radiation Sciences Program managed by Hal Maring.

References

[1] Nieto-Vesperinas M, Dainty JC, editors. Scattering in volumes and surfaces. Amsterdam: North-Holland; 1990.
[2] Sheng P, editor. Scattering and localization of classical waves in random media. Singapore: World Scientific; 1990.
[3] Barabanenkov YuN, Kravtsov YuA, Ozrin VD, Saichev AI. Enhanced backscattering in optics. Progr Opt 1991;29:65–197.
[4] Lagendijk A, van Tiggelen BA. Resonant multiple scattering of light. Phys Rep 1996;270:143–215.
[5] Kuz'min VL, Romanov VP. Coherent phenomena in light scattering from disordered systems. Phys-Uspekhi 1996;39:231–60.
[6] van Rossum MCW, Nieuwenhuizen ThM. Multiple scattering of classical waves: microscopy, mesoscopy, and diffusion. Rev Mod Phys 1999;71:313–71.
[7] Lenke R, Maret G. Multiple scattering of light: coherent backscattering and transmission. In: Brown W, Mortensen K, editors. Scattering in polymeric and colloidal systems. Amsterdam: Gordon and Breach; 2000. p. 1–73.
[8] van Tiggelen BA, Skipetrov SE, editors. Wave scattering in complex media: from theory to applications. Dordrecht, The Netherlands: Kluwer Academic Publishers; 2003.
[9] Mishchenko MI, Travis LD, Lacis AA. Multiple scattering of light by particles: radiative transfer and coherent backscattering. Cambridge: Cambridge University Press; 2006.
[10] Kuga Y, Tsang L, Ishimaru A. Depolarization effects of the enhancement retroreflectance from a dense distribution of spherical particles. J Opt Soc Am A 1985;2:616–8.
[11] Stephen MJ, Cwilich G. Rayleigh scattering and weak localization: effects of polarization. Phys Rev B 1986;34:7564–72.

[12] Akkermans E, Wolf PE, Maynard R, Maret G. Theoretical study of the coherent backscattering of light by disordered media. J Phys (France) 1988;49:77–98.
[13] Shkuratov YuG. A diffraction mechanism for the formation of the opposition effect of the brightness of surfaces having a complex structure. Kinem Fiz Nebes Tel 1988;4(4):33–9 [in Russian].
[14] Mandt CE, Tsang L, Ishimaru A. Copolarized and depolarized backscattering enhancement of random discrete scatters of large size based on second-order ladder and cyclical theory. J Opt Soc Am A 1990;7:585–92.
[15] Muinonen K. Light scattering by inhomogeneous media: backward enhancement and reversal of linear polarization. PhD dissertation. University of Helsinki, Helsinki, 1990.
[16] Mishchenko MI. Polarization effects in weak localization of light: calculation of the copolarized and depolarized backscattering enhancement factors. Phys Rev B 1991;44:12597–600.
[17] Mishchenko MI. Enhanced backscattering of polarized light from discrete random media: calculations in exactly the backscattering direction. J Opt Soc Am A 1992;9:978–82.
[18] Mishchenko MI. Polarization characteristics of the coherent backscatter opposition effect. Earth Moon Planets 1992;58:127–44.
[19] Mishchenko MI. Diffuse and coherent backscattering by discrete random media—I. Radar reflectivity, polarization ratios, and enhancement factors for a half-space of polydisperse, nonabsorbing and absorbing spherical particles. JQSRT 1996;56:673–702.
[20] Wiersma DS, van Albada MP, van Tiggelen BA, Lagendijk A. Experimental evidence for recurrent multiple scattering events of light in disordered media. Phys Rev Lett 1995;74:4193–6.
[21] Mishchenko MI, Travis LD, Lacis AA. Scattering, absorption and emission of light by small particles. Cambridge: Cambridge University Press; 2002 (available in the pdf format at http://www.giss.nasa.gov/~crmim/books.html).
[22] Hovenier JW, Van der Mee C, Domke H. Transfer of polarized light in planetary atmospheres—basic concepts and practical methods. Dordrecht, The Netherlands: Kluwer; 2004.
[23] de Rooij WA. Reflection and transmission of polarized light by planetary atmospheres. PhD dissertation. Vrije Universiteit, Amsterdam, 1985.
[24] Mishchenko MI. Light scattering by randomly oriented axially symmetric particles. J Opt Soc Am A 1991;8:871–82 (Errata: 1992; 9:497).
[25] Waterman PC. Symmetry, unitarity, and geometry in electromagnetic scattering. Phys Rev D 1971;3:825–39.
[26] Mishchenko MI, Hovenier JW. Depolarization of light backscattered by randomly oriented nonspherical particles. Opt Lett 1995;20:1356–8.